International Journal of Multiphase Flow 36 (2010) 293–302

Contents lists available at ScienceDirect

International Journal of Multiphase Flow

journal homepage: www.elsevier.com/locate/ijmulflow

# Prediction of the entrained liquid fraction in vertical annular gas–liquid two-phase flow

Andrea Cioncolini [1], John R. Thome *

*Heat and Mass Transfer Laboratory, École Polytechnique Fédérale de Lausanne, EPFL-STI-IGM-LTCM, Station 9, 1015 Lausanne, Switzerland*

ARTICLE INFO

*Article history:*
Received 23 September 2009
Received in revised form 23 November 2009
Accepted 29 November 2009
Available online 5 December 2009

*Keywords:*
Annular two-phase flow
Entrainment
Entrained liquid fraction
Liquid film atomization

ABSTRACT

The study considers the prediction of the entrained liquid fraction in adiabatic gas–liquid annular two-phase flow in vertical pipes. Nine empirical correlations have been tested against an experimental data bank drawn together in this study containing 1504 points for 8 different gas–liquid combinations and 19 different tube diameters from 5.00 mm to 57.1 mm. The correlation of Sawant, Ishii and Mishima and the one of Oliemans, Pots and Trompé were found to best reproduce the available data. A new correlating approach, derived from both physical intuition and dimensional analysis and capable of providing further physical insight into the liquid film atomization process, was proposed and worked better than any of the existing methods. This new correlation is based on the core flow Weber number that is also a controlling dimensionless group in determining the wall shear stress and associated frictional pressure gradient of annular flows.



## 1. Introduction

Annular two-phase flow, characterized by the presence of a continuous liquid film flowing on the channel wall and surrounding a central gas core laden with entrained liquid droplets, is one of the most frequently observed flow regimes in practical applications involving gas–liquid two-phase flow.

A crucial parameter in the analysis and modeling of annular flows is the fraction of liquid entrained as droplets in the gas core, defined as the ratio of the entrained liquid droplets mass flow rate to the total liquid mass flow rate. The entrained liquid fraction is thus a flow parameter bounded between 0 and 1, with values close to 0 identifying annular flows with an almost perfect segregation between liquid and gas, while a value of 1 corresponds to the disappearance of the liquid film and thus marks the transition from annular flow to dispersed mist flow.

An accurate knowledge of the entrained liquid fraction is essential in most thermal–hydraulics predictions, including the onset of dryout in boiling channels, post-dryout heat transfer and the effectiveness of nuclear reactor core cooling during transient and accident scenarios.

The purpose of the present study is to first assess the accuracy of leading empirical correlations for predicting the entrained liquid fraction, focusing in particular on adiabatic annular two-phase upflow.

An experimental database containing 1504 measurements of the entrained liquid fraction in annular two-phase flow has been collected from the open literature. The database is used to assess the predictive capability of nine empirical correlations of frequent use in practical applications. Finally, a new correlating approach based on both physical intuition and dimensional analysis is proposed, yielding a new correlating equation that outperforms the existing correlations and provides further physical insight into the physics of the liquid entrainment process.

## 2. Experimental database description

The main details regarding the experimental annular flow database collected from the open literature are summarized in Table 1. All data refer to adiabatic gas–liquid (or vapor–liquid) annular two-phase flow through circular pipes in vertical upflow. A flow regime double-check with the flow map of Hewitt and Roberts (1969) is included in Fig. 1. As can be seen, any contamination of the collected data from flow regimes other than annular flow should be negligible. The collected data cover 8 different gas–liquid combinations, including both single-component saturated fluids such as water–steam and refrigerants R113 and R12 and two-component fluids, such as water–air, R140a–air, ethanol–air, water–helium and silicon–air. The experimental data cover 19 different values of tube diameter, ranging from 5.00 mm to 57.1 mm.

Annular two-phase flows can be quite slow in reaching fully developed flow conditions, and some inlet effects can be present

* Corresponding author. Tel.: +41 21 693 5981; fax: +41 21 693 5960.
*E-mail addresses:* andrea.cioncolini@epfl.ch (A. Cioncolini), john.thome@epfl.ch (J.R. Thome).
[1] Tel.: +41 21 693 5984; fax: +41 21 693 5960.

0301-9322/$ - see front matter © 2009 Elsevier Ltd. All rights reserved.
doi:10.1016/j.ijmultiphaseflow.2009.11.011

**Table 1**
Experimental annular flow data bank.

| Reference | Fluids | $d$ (mm) | $P$ (MPa) | $G$ (kgm$^{-2}$ s$^{-1}$) | $x$ | $e$ | $L/d$[b] | No. points |
|---|---|---|---|---|---|---|---|---|
| Whalley et al. (1974)[a] | $H_2O$–air<br>R140a–air | 31.8 | 0.10–0.30 | 79–792 | 0.10–0.90 | 0.15–0.96 | 590 | 158 |
| Gill et al. (1964, 1969)[a] | $H_2O$–air | 31.8 | 0.10–0.30 | 44–246 | 0.12–0.88 | 0.03–0.70 | 167–520 | 43 |
| Brown (1978)[a] | $H_2O$–air | 31.8 | 0.17–0.31 | 160–320 | 0.33–0.66 | 0.42–0.86 | 420 | 30 |
| Cousins et al. (1965)[a], Cousins and Hewitt (1968a,b)[a] | $H_2O$–air | 9.53;31.8 | 0.14–0.41 | 107–477 | 0.15–0.82 | 0.03–0.65 | 230–480 | 123 |
| Minh and Huyghe (1965)[a] | $H_2O$–air<br>Ethanol–air | 6.00;12.0 | 0.20–0.80 | 112–1293 | 0.03–0.90 | 0.02–0.87 | na | 102 |
| Hewitt and Pulling (1969)[a] | $H_2O$–steam | 9.30 | 0.24–0.45 | 297 | 0.14–0.75 | 0.01–0.68 | 390 | 72 |
| Keeys et al. (1970)[a] | $H_2O$–steam | 12.6 | 3.5–6.9 | 1313–2763 | 0.25–0.68 | 0.65–0.86 | 290 | 18 |
| Singh et al. (1969)[a] | $H_2O$–steam | 12.5 | 6.9–8.3 | 518–973 | 0.27–0.93 | 0.12–0.82 | 180 | 39 |
| Würtz (1978)[a] | $H_2O$–steam | 10.0;20.0 | 3.0–9.0 | 500–3000 | 0.08–0.70 | 0.12–0.92 | 450–900 | 93 |
| Nigmatulin et al. (1977)[a] | $H_2O$–steam | 13.3 | 1.0–10.0 | 500–4000 | 0.10–0.90 | 0.07–0.98 | 300 | 45 |
| Lopez de Bertodano et al. (2001) | R113 | 10.0 | 0.32–0.53 | 205–1089 | 0.35–0.90 | 0.18–0.90 | 350 | 48 |
| Han et al. (2007) | $H_2O$–air | 9.52 | 0.10 | 182–347 | 0.10–0.28 | 0.02–0.07 | 166 | 30 |
| Okawa et al. (2005) | $H_2O$–air | 5.00 | 0.10–0.76 | 265–1939 | 0.05–0.77 | 0.05–0.70 | 320 | 170 |
| Sawant et al. (2008) | $H_2O$–air | 9.40 | 0.10–0.40 | 123–968 | 0.09–0.90 | 0.08–0.75 | 210 | 59 |
| Jepson et al. (1989) | $H_2O$–air<br>$H_2O$–He | 10.3 | 0.15 | 54–221 | 0.07–0.75 | 0.01–0.26 | 291 | 49 |
| Azzopardi and Zaidi (2000) | $H_2O$–air | 38.0 | 0.15 | 47–155 | 0.21–0.73 | 0.12–0.50 | 118 | 28 |
| Wallis (1962) | $H_2O$–air<br>Silicon–air | 15.9 | 0.10–0.40 | 58–374 | 0.04–0.73 | 0.01–0.90 | na | 112 |
| Schadel et al. (1990) | $H_2O$–air | 25.4;42.0;57.1 | 0.15 | 51–316 | 0.35–0.91 | 0.10–0.77 | 150 | 64 |
| Jagota et al. (1973) | $H_2O$–air | 25.4 | 0.20–0.40 | 135–591 | 0.12–0.69 | 0.05–0.54 | 150–261 | 76 |
| Mayinger and Langner (1976) | R12 | 14.0 | 1.10 | 300–1000 | 0.30–0.90 | 0.05–0.80 | 357 | 16 |
| Hinkle (1967) | $H_2O$–air | 12.6 | 0.20–0.60 | 150–730 | 0.14–0.71 | 0.02–0.46 | 121–262 | 129 |

[a] Data included in the AERE Harwell data bank.
[b] Distance of test section inlet from mixer (two-component flows) or preheater (saturated flows).

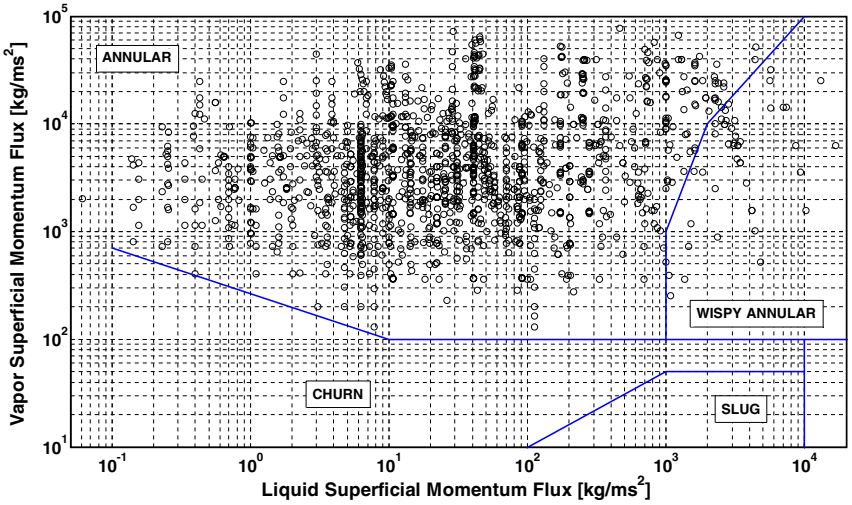


**Fig. 1.** Flow regime double-check.

up to 100–300 tube diameters from the inlet (Wolf et al., 2001). As can be seen from Table 1, most of the experimental rigs have been designed with calming sections long enough to significantly damp out any dependence on inlet conditions. As such, inlet effects are not considered in the present study.

The most frequently used experimental techniques for measuring the entrained liquid fraction are the liquid film removal method and the sampling method. In the liquid film removal method, the annular liquid film is extracted from the test tube, typically through a porous wall section, together with a fraction of the gas flow rate. During the tests, the amount of mixture extracted is gradually increased, while the extracted mass flow rates of both liquid and gas are measured at each stage. If the measurements are plotted as extracted liquid mass flow rate versus extracted gas mass flow rate, the data typically show a plateau, which is normally identified as the liquid film mass flow rate. Unfortunately, the plateau is not always well pronounced (Azzopardi and Zaidi, 2000), so that the results can be somewhat subjective and not that accurate. Also, Sekoguchi and Tanaka (1985) noted a potential effect of the extraction porous tube length on the results. As the liquid film flows over the porous surface through which it is being sucked out, its thickness decreases, and so does the entrainment, while the deposition of droplets from the core flow continues. As such, a long extraction tube is likely to perturb the annular flow that is being analyzed, thus affecting the measurements. On the other hand, a short extraction tube would minimize the perturbation of the flow, at the expense of a potential incomplete extraction of the liquid film. In the sampling probe method, a small diameter sampling tube facing upstream is inserted into the test section and part of the core flow is sucked out. Gas and

entrained droplets are then separated and their mass flow rates measured. The process is repeated at a suitable number of points in the radial direction in the pipe cross-section, and the entrained liquid mass flow rate is finally estimated from integrating the local values obtained. The greatest difficulty in using the sampling probe method is the determination of the location of the interface between gas core and liquid film, which normally is wavy. If the sampling probe is set too close to the interface, it may pick up liquid from the crests of the waves travelling on the liquid film, thus affecting the measurements. Besides, when measuring low entrained liquid fraction values, the evaporation of the collected droplets may affect the measurements (Azzopardi and Zaidi, 2000). Further experimental techniques of less frequent use for measuring the entrained liquid fraction are the optical method and the tracer method. In the optical method, used by Azzopardi and Zaidi (2000), the liquid film is removed through a porous wall and the droplet concentration in the gas core is deduced from the scattering of a beam of light shown through the cloud of droplets. In the tracer method, used by Jagota et al. (1973) and by Han et al. (2007) together with a specially designed liquid–gas separator, a tracer liquid is introduced into the liquid film. The fraction of liquid entrained is then deduced from monitoring the tracer concentration downstream of the injection point.

In conclusion, measuring the entrained liquid fraction is a very challenging task. The most frequently used experimental techniques are quite invasive and can significantly perturb the annular two-phase flow that is being analyzed. As such, a part of the available experimental data might be affected by considerable uncertainties, and significant scatter can be expected when merging data from different studies.

## 3. Empirical correlations

In this study, the correlations of Paleev and Filippovich (1966), Wallis (1968), Oliemans et al. (1986), Ishii and Mishima (1989), Nakazatomi and Sekoguchi (1996), Utsuno and Kaminaga (1998), Pan and Hanratty (2002) and Sawant et al. (2008, 2009) are considered. In what follows, the correlations of Oliemans et al. (1986) and the correlation of Sawant et al. (2009), which will be shown to best reproduce the available database, are discussed. Further details on the other correlations and their implementation can be found in the Electronic Annex in the online version of this article.

According to Oliemans et al. (1986), the entrained liquid fraction $e$ is predicted as follows:

$$\frac{e}{1-e} = 10^{b_0}\rho_l^{b_1}\rho_g^{b_2}\mu_l^{b_3}\mu_g^{b_4}\sigma^{b_5}d^{b_6}J_l^{b_7}J_g^{b_8}g^{b_9} \tag{1}$$

where $\rho_l$, $\rho_g$, $\mu_l$ and $\mu_g$ are the liquid and vapor densities and viscosities, respectively, $\sigma$ is the surface tension, $d$ is the tube diameter, $g$ is the acceleration of gravity and $J_l$ and $J_g$ are the superficial liquid and gas velocities:

$$J_l = \frac{(1-x)G}{\rho_l}; \quad J_g = \frac{xG}{\rho_g} \tag{2}$$

where $x$ is the vapor quality and $G$ is the total mass flux. The exponents $b_0$–$b_9$ appearing in Eq. (1) are summarized in Table 2 as function of the liquid film Reynolds number, which is defined as follows:

$$\mathrm{Re}_{lf} = (1-e)(1-x)\frac{Gd}{\mu_l} \tag{3}$$

A constraint to the values of the exponents $b_0$–$b_9$ in Eq. (1) is that the right-hand side of Eq. (1) forms a dimensionless group. As can be seen in Eq. (3), the liquid film Reynolds number depends on the fraction of liquid entrained $e$, so that an iterative calculation is required. Operatively, a first order estimate for $e$ is obtained using the values $b_0$–$b_9$ from Table 2 which are applicable irrespective of the liquid film Reynolds number. The Reynolds number of the liquid film can then be calculated, and the estimate for $e$ accordingly refined. The procedure is then repeated, with 2–3 steps typically required to converge.

In the method proposed by Sawant et al. (2009), the entrained liquid fraction $e$ is predicted as follows:

$$\frac{e}{e_{\max}} = \tanh\left[2.31\times10^{-4}Re_l^{-0.35}(We - We_{crit})^{1.25}\right] \tag{4}$$

where the maximum entrained liquid fraction $e_{\max}$ is calculated as:

$$e_{\max} = 1 - \frac{13N_\mu^{-0.5} + 0.3(Re_l - 13N_\mu^{-0.5})^{0.95}}{Re_l} \tag{5}$$

The viscosity number $N_\mu$, the liquid Reynolds number $Re_l$ and the Weber number $We$ are defined as:

$$N_\mu = \mu_l\left(\rho_l\sigma\sqrt{\frac{\sigma}{g(\rho_l-\rho_g)}}\right)^{-0.5}; \quad Re_l = \frac{\rho_l J_l d}{\mu_l};$$
$$We = \frac{\rho_g J_g^2 d}{\sigma}\left(\frac{\rho_l-\rho_g}{\rho_g}\right)^{0.25} \tag{6}$$

The critical Weber number $We_{crit}$ is calculated as indicated in Eq. (6), where the following critical superficial gas velocity $J_{gcrit}$ is used in place of the superficial gas velocity $J_g$:

$$J_{gcrit} = \frac{11.78Re_l^{-0.3}N_\mu^{0.8}}{\frac{\mu_l}{\sigma}\sqrt{\frac{\rho_g}{\rho_l}}} \iff Re_l \leqslant 1635$$
$$J_{gcrit} = \frac{N_\mu^{0.8}}{\frac{\mu_l}{\sigma}\sqrt{\frac{\rho_g}{\rho_l}}} \iff Re_l \geqslant 1635 \tag{7}$$

Besides using empirical correlations, the entrained liquid fraction can also be predicted with mechanistic models, where the rate of liquid atomization from the liquid film and the rate of droplet deposition onto the liquid film are separately modeled. Although mechanistic models are not explicitly considered in the present study, some limited assessment of existing correlations for predicting the rates of entrainment and deposition is provided in the Electronic Annex available in the online version of this paper.

**Table 2**
Parameters for Oliemans et al. correlation.

| $Re_{lf}$ | $b_0$ | $b_1$ | $b_2$ | $b_3$ | $b_4$ | $b_5$ | $b_6$ | $b_7$ | $b_8$ | $b_9$ |
|---|---|---|---|---|---|---|---|---|---|---|
| All values | −2.52 | 1.08 | 0.18 | 0.27 | 0.28 | −1.80 | 1.72 | 0.70 | 1.44 | 0.46 |
| $10^2$–$3\times10^2$ | −0.69 | 0.63 | 0.96 | −0.80 | 0.09 | −0.88 | 2.45 | 0.91 | −0.16 | 0.86 |
| $3\times10^2$–$10^3$ | −1.73 | 0.94 | 0.62 | −0.63 | 0.50 | −1.42 | 2.04 | 1.05 | 0.96 | 0.48 |
| $10^3$–$3\times10^3$ | −3.31 | 1.15 | 0.40 | −1.02 | 0.46 | −1.00 | 1.97 | 0.95 | 0.78 | 0.41 |
| $3\times10^3$–$10^4$ | −8.27 | 0.77 | 0.71 | −0.13 | −1.18 | −0.17 | 1.16 | 0.83 | 1.45 | −0.32 |
| $10^4$–$3\times10^4$ | −6.38 | 0.89 | 0.70 | −0.17 | −0.55 | −0.87 | 1.67 | 1.04 | 1.27 | 0.07 |
| $3\times10^4$–$10^5$ | −0.12 | 0.45 | 0.25 | 0.86 | −0.05 | −1.51 | 0.91 | 1.08 | 0.71 | 0.21 |

## 4. Results

The comparison of the measured entrained liquid fraction data versus the empirical correlation predictions is presented in the Figures included in the Electronic Annex in the online version of this article. Here, Figs. 6 and 7 to be discussed later on show the results for the best two methods. The statistical comparisons between measured data and predictions are reported in Tables 3 and 4. In Table 3, in particular, the entire databank is considered, while Table 4 is limited to entrained liquid fraction values above 0.5 (478 points out of a total of 1504, corresponding to 31.8% of the entire databank). The threshold of 0.5 used here is selected to segregate annular flows where the majority of the liquid phase is transported as entrained droplets, with the purpose to assess the correlations predictive capability not only in general terms but also in situations of potential interest for dryout prediction and modeling. Different thresholds, such as 0.4 or 0.6, yield similar results (the corresponding Tables with the statistical comparisons are included in the Electronic Annex in the online version of this article). Thresholds bigger than 0.6 do not allow the segregation of enough data for a significant assessment. In the present study, the empirical correlations are ranked on the basis of their mean absolute percentage error. If two correlations yield comparable values of the mean absolute percentage error (difference within ±1%), then the ranking is done according to the percentage of data captured within ±15%,±30% and ±50%. From inspection of Table 3, covering the entire database, it can be seen that the best predictions are given by the correlation of Sawant et al. (2009), with a mean absolute percentage error of 35.0% and almost 6 points out of 10 predicted to within ±30%, followed by the correlation of Ishii and Mishima (1989) and that of Pan and Hanratty (2002). From inspection of Table 4 with entrained liquid fraction values above 0.5, on the other hand, the best predictions are given by the correlation of Oliemans et al. (1986), with a mean absolute percentage error of 17.3% and 8 points out of 10 predicted to within ±30%, followed by the correlations of Sawant et al. (2008, 2009).

## 5. New prediction method

In what follows, a new correlating approach for the entrained liquid fraction is proposed. In particular, the new correlation is derived heuristically using physical intuition. Successively, in Section 6, dimensional analysis will be used to refine the results and better support the conclusions already obtained.

Annular two-phase flows can be regarded as a special form of a liquid atomization process, where a high velocity confined spray, composed by the gas and entrained liquid droplets, flows in the center of the channel dragging and atomizing an annular liquid film that slides along the channel wall. Liquid atomization processes are frequently used in industry, anytime it is required to increase the interfacial area to enhance the transfer processes that take place across the gas–liquid interface, and as such have been extensively investigated. Liquid atomization processes differ typically in the way the energy required to drive the liquid disintegration is provided. Of special interest here for annular two-phase flow modeling is the liquid atomization induced by the interaction of the liquid with a high velocity gas stream, which provides the energy for the liquid disintegration in the form of kinetic energy. Although these kind of liquid atomization processes are considerably complicated and possibly not yet completely clarified, it is commonly accepted that the liquid–gas aerodynamic interaction plays a major role in the liquid disintegration process (Reitz and Bracco, 1982; Crowe, 2006). The dimensionless group that is typically used to capture the aerodynamic interaction is a Weber number, which represents the ratio of the disrupting aerodynamic force to the surface tension retaining force. In the case of a liquid circular jet atomized by a coaxial gas stream, for example, the Weber number would take the following form:

$$We = \frac{\rho_g V_{rel}^2 d_{jet}}{\sigma} \tag{8}$$

where $\rho_g$ is the gas density, $V_{rel}$ is the relative velocity between the gas stream and the liquid jet and $d_{jet}$ is the jet diameter. As such, assuming that an annular flow can be regarded as a particular form of liquid atomization process mostly induced by the aerodynamic interaction of the droplet-laden gas core with the liquid film, a potentially good candidate to correlate the entrained liquid fraction would be a properly defined Weber number. As a matter of fact, the majority of the empirical correlations considered here make use of a Weber number in some form. In the present study, in particular, the following form of the Weber number is considered, namely the core flow Weber number:

$$We_c = \frac{\rho_c V_c^2 d_c}{\sigma} \tag{9}$$

where $\rho_c$ is the droplet-laden gas core density, $V_c$ is the core flow velocity and $d_c$ is the core flow hydraulic diameter. This form of the Weber number was found to be the controlling dimensionless group in determining annular flow wall shear and frictional pressure gradient (Cioncolini et al., 2009b), so that its use here appears to be a promising starting point. As described by Cioncolini et al. (2009b), the accurate evaluation of the core flow Weber number $We_c$ requires the estimate of the average liquid film thickness. According to them, however, a simplified but reasonably accurate estimate can be obtained from the void fraction $\varepsilon$ and the liquid droplet hold-up $\gamma$ values. In particular, the core flow hydraulic diameter $d_c$ can be calculated as follows:

$$d_c \approx d\sqrt{\varepsilon + \gamma - \varepsilon\gamma} \tag{10}$$

where $d$ is the tube diameter. As schematically indicated in Fig. 2, the void fraction $\varepsilon$ represents the fraction of the channel cross-sectional area occupied by the gas phase, while the liquid droplet hold-up $\gamma$ represents the fraction of the liquid phase cross-sectional area occupied by the entrained droplets. The void fraction $\varepsilon$ is predicted according to Woldesemayat and Ghajar (2007):

$$\varepsilon = \frac{J_g}{C_0 J_g + V_{drift}}; \quad C_0 = 1 + \left(\frac{J_l}{J_g}\right)^n; \quad n = \left(\frac{\rho_g}{\rho_l}\right)^{0.1}$$
$$V_{drift} = 2.9\left[\frac{gd\sigma(1+\cos\theta)(\rho_l - \rho_g)}{\rho_l^2}\right]^{0.25}(1.22 + 1.22\sin\theta)^{\frac{P_{atm}}{P}} \tag{11}$$

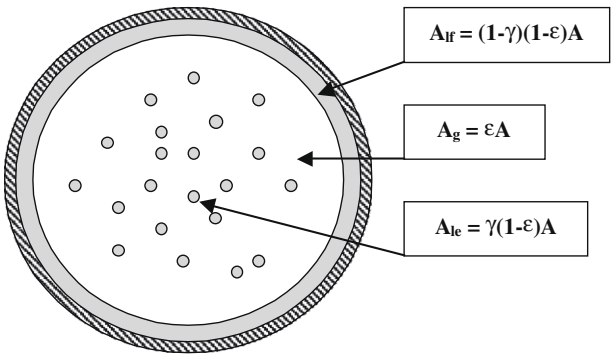


**Fig. 2.** Schematic representation of the cross-sectional area A split among the phases.

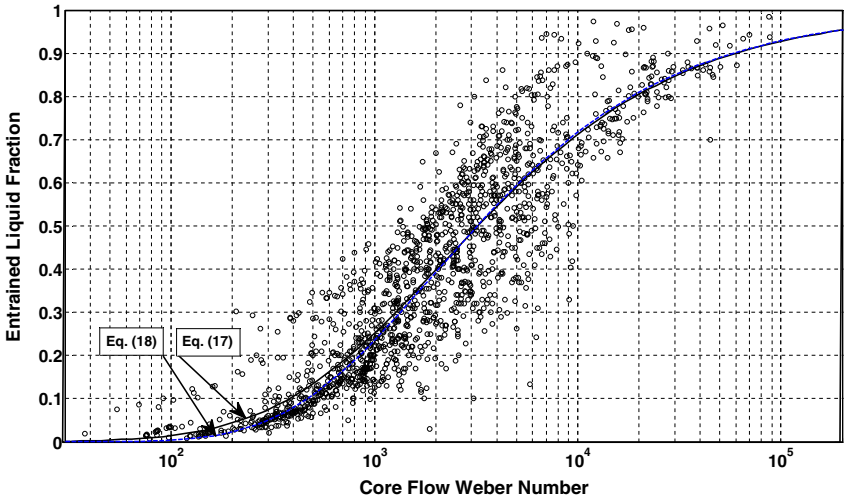


**Fig. 3.** Entrained liquid fraction vs. core flow Weber number.

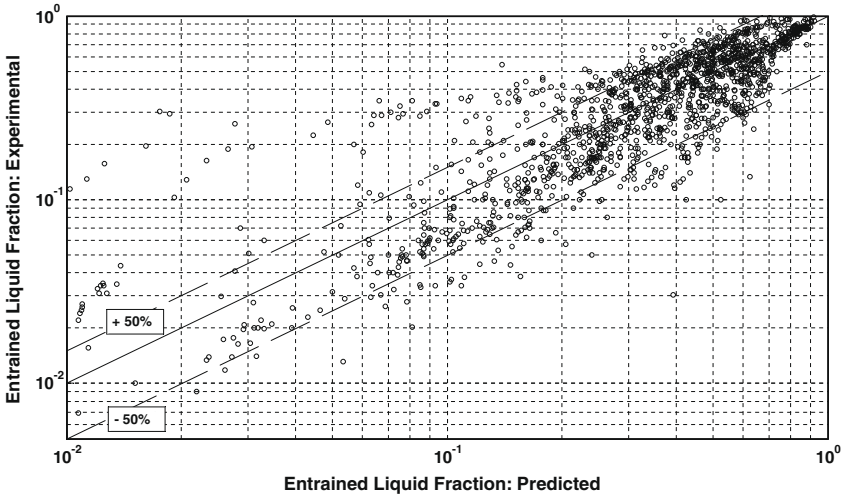


**Fig. 4.** Entrained liquid fraction: measured data vs. predictions of Eq. (17).

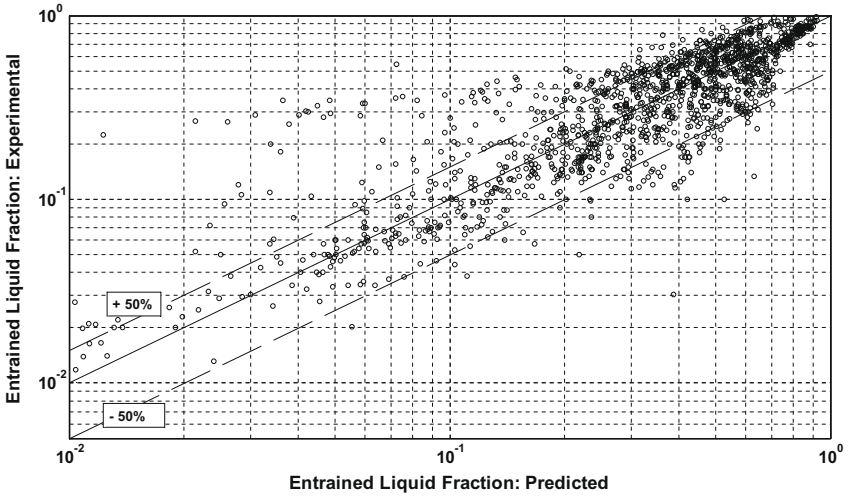


**Fig. 5.** Entrained liquid fraction: measured data vs. predictions of Eq. (18).

where the numerical constant 2.9 appearing in Eq. (11) has the dimension $m^{-0.25}$, $\theta$ is the channel inclination angle ($\theta = 0$ for horizontal flow), $P_{atm}$ is atmospheric pressure and $P$ is the system pressure. The liquid droplet hold-up $\gamma$ is estimated neglecting the slip

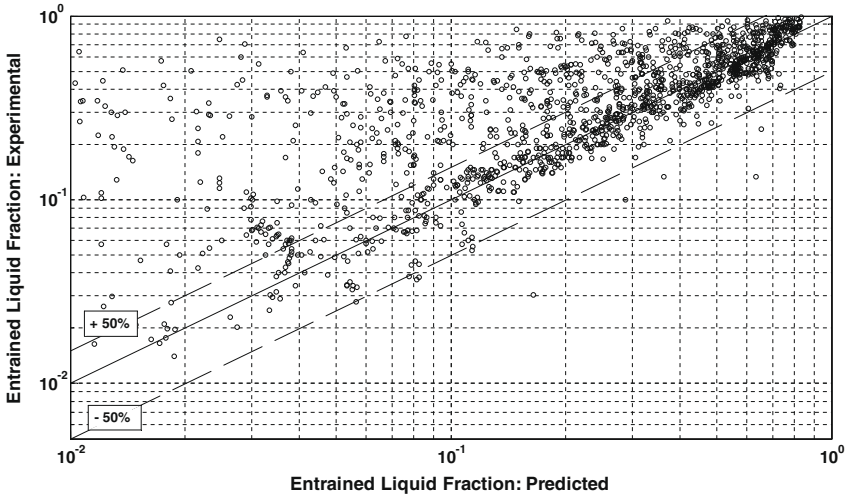


**Fig. 6.** Entrained liquid fraction: measured data vs. predictions of Sawant et al. (2009) correlation, Eq. (4).

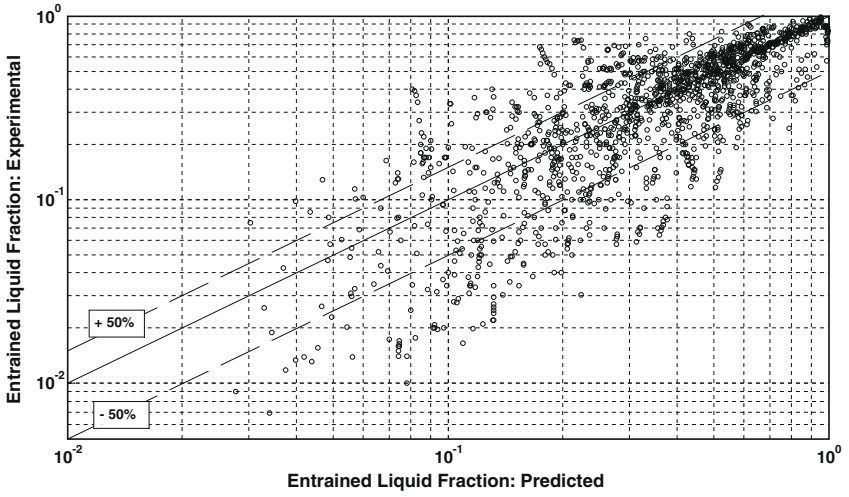


**Fig. 7.** Entrained liquid fraction: measured data vs. predictions of Oliemans et al. (1986) correlation, Eq. (1).

**Table 3**
Statistical comparison between experimental data and correlations: entire database (1504 points).

| | (1) | (2) | (3) | (4) | (5) |
|---|---|---|---|---|---|
| Oliemans et al. (1986) | 56.7 | −46.1 | 35.2 | 51.8 | 69.7 |
| Ishii and Mishima (1989) | 37.8 | −2.9 | 29.6 | 55.5 | 75.1 |
| Paleev and Filippovich (1966) | 193 | −137 | 12.2 | 23.8 | 33.4 |
| Wallis (1968) | 94.8 | −73.4 | 15.3 | 29.1 | 46.3 |
| Nakazatomi and Sekoguchi (1996) | 192 | −161 | 7.2 | 16.6 | 33.6 |
| Pan and Hanratty (2002) | 40.4 | 33.1 | 28.5 | 54.8 | 72.7 |
| Sawant et al. (2008) | 42.8 | −4.7 | 37.4 | 56.9 | 74.8 |
| Sawant et al. (2009) | 35.0 | 21.5 | 35.8 | 57.7 | 71.1 |
| Utsuno and Kaminaga (1998) | 217 | 209 | 9.3 | 11.5 | 15.5 |
| Present study Eq. (17) | 40.4 | −17.4 | 31.4 | 54.4 | 73.1 |
| Present study Eq. (18) | 35.6 | −6.0 | 34.6 | 59.8 | 78.4 |

(1) – Mean absolute percentage error (%) $\frac{100}{n}\sum_1^n \frac{|e_{exp}-e_{cal}|}{e_{exp}}$.
(2) – Mean percentage error (%) $\frac{100}{n}\sum_1^n \frac{e_{exp}-e_{cal}}{e_{exp}}$.
(3) – Percentage of experimental data within ±15%.
(4) – Percentage of experimental data within ±30%.
(5) – Percentage of experimental data within ±50%.

**Table 4**
Statistical comparison between experimental data and correlations: entrained liquid fraction values $e$ above 0.5 (478 points out of 1504, 31.8% of entire database).

| | (1) | (2) | (3) | (4) | (5) |
|---|---|---|---|---|---|
| Oliemans et al. (1986) | 17.3 | 10.3 | 58.6 | 81.2 | 92.0 |
| Ishii and Mishima (1989) | 29.4 | −8.0 | 27.8 | 60.5 | 84.1 |
| Paleev and Filippovich (1966) | 48.9 | 9.5 | 19.5 | 39.1 | 55.4 |
| Wallis (1968) | 31.6 | −7.6 | 22.0 | 49.4 | 81.8 |
| Nakazatomi and Sekoguchi (1996) | 44.7 | −3.0 | 10.2 | 27.8 | 58.6 |
| Pan and Hanratty (2002) | 30.6 | 28.3 | 31.0 | 63.6 | 80.7 |
| Sawant et al. (2008) | 25.2 | 17.2 | 48.3 | 66.9 | 82.2 |
| Sawant et al. (2009) | 27.5 | 23.4 | 43.9 | 65.7 | 79.7 |
| Utsuno and Kaminaga (1998) | 71.9 | 69.6 | 24.3 | 27.0 | 29.9 |
| Present study Eq. (17) | 15.9 | 10.9 | 52.3 | 87.9 | 99.4 |
| Present study Eq. (18) | 16.2 | 10.8 | 52.1 | 87.4 | 99.2 |

(1) – Mean absolute percentage error (%) $\frac{100}{n}\sum_1^n \frac{|e_{exp}-e_{cal}|}{e_{exp}}$.
(2) – Mean percentage error (%) $\frac{100}{n}\sum_1^n \frac{e_{exp}-e_{cal}}{e_{exp}}$.
(3) – Percentage of experimental data within ±15%.
(4) – Percentage of experimental data within ±30%.
(5) – Percentage of experimental data within ±50%.

between the entrained liquid droplets and the carrier gas phase as follows:

$$\gamma = e\frac{\varepsilon}{1-\varepsilon}\frac{1-x}{x}\frac{\rho_g}{\rho_l} \tag{12}$$

The core flow velocity $V_c$ is calculated as follows:

$$V_c = \frac{[x+e(1-x)]G}{\rho_c}\left(\frac{d}{d_c}\right)^2 \tag{13}$$

Finally, the core flow density $\rho_c$ is calculated as:

$$\rho_c = (1-\varepsilon_c)\rho_l + \varepsilon_c\rho_g; \quad \varepsilon_c = \frac{\varepsilon}{\varepsilon+\gamma(1-\varepsilon)} \tag{14}$$

where $\varepsilon_c$ is the droplet-laden gas core void fraction.

The measured entrained liquid fraction values are displayed in Fig. 3 versus the core flow Weber number $We_c$ (a further plot that differentiates among the different contributors to the experimental databank is included in the Electronic Annex in the online version of this article). As can be seen, the scatter in the data is significant, as expected due to the already highlighted difficulties in performing entrainment measurements. Nonetheless, the data points cluster reasonably well, clearly indicating a dependence of the entrained liquid fraction on the core flow Weber number. In particular, the measured data in Fig. 3 appear to collapse on a sigmoid trend.

Sigmoid trends typically describe the evolution of dynamic systems characterized by a positive feedback in their early evolution, giving rise to an exponential growth, followed by a negative feedback in their later stage of evolution that damps the rate of growth and brings the system to saturation. In the present case, in particular, the sigmoid trend in Fig. 3 can be interpreted as follows. For low values of the core flow Weber number $We_c$, the entrained liquid fraction $e$ is very small, and the annular flow exhibits an almost perfect segregation between the phases. As $We_c$ increases, $e$ also increases, yielding an increase of the core flow density and kinetic energy which, in turn, enhance the liquid atomization and trigger a further increase in $e$. A positive feedback sets up giving rise to the initial exponential growth that can be seen in Fig. 3. As $e$ increases, the liquid film thickness decreases, leading eventually to a decrease of liquid atomization, since less and less liquid is left available for further atomization. A negative feedback then sets up, damping the system and bringing it to saturation for high $We_c$ values, as can be seen in Fig. 3. A good candidate to capture a sigmoid trend and thus provide a correlation between $e$ and $We_c$ is the generalized logistic function (Jukić and Scitovski, 1996), which for a target variable bounded between 0 and 1 as $e$ in the present case is a three parameter function that reads as follows:

$$e = (1+be^{-cgx})^{-\frac{1}{g}}; \quad b,c,g>0 \tag{15}$$

where $c$ is the growth rate, $b$ is related to the abscissa of maximum growth and $g$ is an asymmetry coefficient. Generalized logistic functions, such as Eq. (15), find applications as fitting functions in a wide range of fields including biology, biomathematics, demography, economics, chemistry, statistics, medicine and artificial intelligence. Besides the generalized logistic function used here, however, other functions can be used to reproduce a sigmoid trend, such as the hyperbolic tangent (used, among others, by Sawant et al. (2008, 2009)), the arctangent, the Gompertz curve, several algebraic functions and also the cumulative distribution function of some frequently used probability distributions. As such, the selection of an 'S' shaped fitting function among the ones available is largely a matter of personal choice and convenience.

Keeping in mind that in Fig. 3 the $x$-axis is reported in logarithmic scale, the use of Eq. (15) in the present context yields the following correlating equation for the entrained liquid fraction:

$$e = (1+bWe_c^{-d})^{-\frac{1}{g}}; \quad d = \frac{cg}{\ln(10)} \tag{16}$$

where the parameters $b$, $c$ and $g$ have to be determined from the experimental data solving a non-linear regression problem. If the method of least-squares is used in fitting the data, then the parameters are found minimizing the sum of the squares of the residuals, yielding the following correlating equation:

$$e = \left(1+48.22We_c^{-0.671}\right)^{-3.582} \tag{17}$$

From inspecting Fig. 3 it can be seen that in the region of low entrained liquid fraction values most of the data points cluster together. Some points, however, although exhibiting a similar trend to that of the rest of the data, are considerably shifted toward higher values of the entrained liquid fraction. These points might be regarded as potential outliers, i.e. observations that are significantly distant from the rest of the data and that, therefore, appear inconsistent with the remainder of the data set. It is worth highlighting that at present there is no 'rigid' mathematical definition of what constitutes an outlier, so that determining whether or not an observation is an outlier is ultimately a subjective exercise. Traditionally, the classical approach was to manually screen the databank to remove any potential outlier. Besides being questionable, since identifying an outlier is somewhat subjective, the classical approach is becoming impractical as experimental databanks are becoming larger and larger.

The main disadvantage of least-squares fitting is its high sensitivity to outliers. Outliers have a large influence on the fit because squaring the residuals magnifies the effect of these extreme points, so that even a few outliers can dramatically affect a least-squares fit. One possibility to mitigate the outliers influence is the use of weighted least-squares fitting: each data point in the database is given a weight that is successively used in the least-squares regression. Ideally, these weights should reflect the quality of the data, and should therefore be related to the experimental uncertainty of the measurements. Unfortunately, however, for most of the collected data the experimental uncertainties are not available. Another possibility to minimize the influence of outliers is the use of robust regression fitting techniques, instead of least-squares fitting. Robust fitting techniques are forms of regression analysis designed to circumvent some of the limitations of the traditional least-squares technique, specifically the sensitivity to outliers. This is done using different, more appropriate metrics to evaluate the distance between observations and predictions. Although computationally more demanding than traditional techniques, robust regression methods are expected to come into wider use in the near future, due to their superior performance with respect to least-squares estimates in many practical situations. As a matter of fact, most statistical software packages already implement robust fitting techniques (the results presented in this study have been obtained within the MATLAB numerical computing environment, using built-in features only). In particular, the robust method of least-absolute-residuals is used here. Instead of minimizing the sum of the squares of the residuals, as it is done with least-squares methods, this method minimizes the sum of the absolute values of the residuals, so that extreme points have less influence on the fit. This yields the following correlating equation:

$$e = \left(1+13.18We_c^{-0.655}\right)^{-10.77} \tag{18}$$

The exponent of 10.77 might look somewhat large, in the context of typical two-phase flow correlations. It is worth remembering, however, that the purpose of this coefficient is to massage the asymmetry of the sigmoid curve, so that mathematically it is only required to be strictly positive.

Both Eqs. (17) and (18) are displayed in Fig. 3, showing a reasonably good fit of the data. In particular, both equations provide almost identical results for entrained liquid fraction values above ≈0.3, suggesting that in this region of the database the data points are quite scattered but should not include outliers. In the region of entrained liquid fraction values below ≈0.3, however, the correlation obtained with robust regression, Eq. (18), appears to better follow the bulk of the data.

The comparison of the measured data with the predictions of Eqs. (17) and (18) is presented in Figs. 4 and 5, respectively, while the statistical comparison between measured data and predictions is reported in Tables 3 and 4. Also included in Figs. 6 and 7 is the comparison of the measured data with the predictions of the correlation of Sawant et al. (2009), Eq. (4), and with the predictions of the correlation of Oliemans et al. (1986), Eq. (1). Further plots are included in the Electronic Annex in the online version of this article. In Table 3 it can be seen that Eq. (18) fits the data slightly better than the other correlations tested, with a mean absolute percentage error of 35.6% and 6 points out of 10 predicted to within ±30%. Besides, Eq. (18) obtained with robust regression significantly outperforms Eq. (17) obtained with standard least-squares fitting, clearly showing the superiority of robust techniques in dealing with large, highly scattered databanks potentially affected by outlier contamination. In Table 4 it can be seen that both Eqs. (17) and (18) provide almost identical results and both perform better than all the other correlations tested, with a mean absolute percentage error around 16.0% and almost 9 points out of 10 predicted to within ±30%.

Direct comparison of Eqs. (17) and (18) with other correlations is somewhat unfair, since both Eqs. (17) and (18) have been designed with the present databank while all other correlations are based on different data sets. Nonetheless, the good correlating capability of Eqs. (17) and (18) suggests that, within the limits of the present study, an annular flow can be regarded as a pseudo liquid atomization process, where the liquid film disintegration is mostly related with the aerodynamic interaction of the liquid film and the droplet-laden gas core, which seems to be properly captured by the core flow Weber number. It is worth highlighting that this same core flow Weber number already proved to be the most influential dimensionless group in determining annular flow shear stress and frictional pressure gradient (Cioncolini et al., 2009b), so that this form of the Weber number seems to capture a good deal of information regarding annular flows.

Finally, the correlating equations proposed here are much simpler than existing ones, as they depend on one dimensionless group only, but this formal simplicity, unfortunately, comes at the expense of their ease of use. Both Eqs. (17) and (18), in fact, have to be used iteratively, since the core flow Weber number depends on the entrained liquid fraction. This, of course, allows the intrinsic non-linearity of the entrainment process to be properly reproduced. Operatively, a guess value for the entrained liquid fraction is selected (such as $10^{-3}$), the core flow Weber number is calculated and the estimate of the entrained liquid fraction correspondingly refined. The procedure is then repeated, with 5–10 steps typically required to converge (to within 1–2%).

## 6. Dimensional analysis

So far, the analysis has been conducted heuristically on the basis of physical intuition. In particular, the core flow Weber number has been identified as a potentially good candidate for modeling the liquid film atomization process and to correlate the entrained liquid fraction data. Although Fig. 3 seems to support this conclusion, other dimensionless groups might do better than the core flow Weber number or might be used in conjunction with the core flow Weber number to improve the predictive capability of the proposed correlations, Eqs. (17) and (18). In what follows, therefore, dimensional analysis is used to provide further support to the conclusions already drawn and to possibly improve the correlating equation proposed.

The entrained liquid fraction $e$ can be assumed to depend on the densities $\rho_l$ and $\rho_c$ and the viscosities $\mu_l$ and $\mu_c$ of the liquid and the droplet-laden gas core, on the surface tension $\sigma$, on the mean velocities of the liquid film $V_l$ and the gas core $V_c$, on the average liquid film thickness $t$ and on the core flow diameter $d_c$ as follows:

$$e = e(\rho_l, \rho_c, \mu_l, \mu_c, \sigma, V_l, V_c, d_c, t) \tag{19}$$

The influential parameters included in Eq. (19) are similar to the ones proposed by Oliemans et al. (1986), Eq. (1). A notable difference is the use of the density $\rho_c$ and the viscosity $\mu_c$ of the droplet-laden core flow instead of the density $\rho_g$ and the viscosity $\mu_g$ of the gas, allowing the feedback of the entrainment process on the core flow properties to be properly captured. Besides, the mean velocities $V_l$ and $V_c$ are used here in place of the superficial velocities $J_l$ and $J_g$ and two length scales $t$ and $d_c$ are introduced in place of the tube diameter $d$. This list of influential parameters included in Eq. (19) is not claimed to be complete but should, nonetheless, include all the essential physical properties of annular two-phase flows. All these influential parameters are calculated as follows. The mean velocities of the liquid film $V_l$ and the gas core $V_c$ are calculated as:

$$V_l = \frac{(1-e)(1-x)Gd^2}{4\rho_l t(d-t)}; \quad V_c = \frac{[x+e(1-x)]G}{\rho_c}\left(\frac{d}{d_c}\right)^2 \tag{20}$$

The average liquid film thickness $t$ is estimated by numerically integrating the mass conservation equation for the liquid film:

$$(1-e)(1-x)\Gamma = 2\pi\rho_l \int_0^t V_{lf}(y)(R-y)dy \tag{21}$$

where $\Gamma$ is the total mass flow rate, $R$ and $y$ are the tube radius and the distance from the tube wall, respectively, and the velocity profile in the liquid film $V_{lf}$ is estimated according to Cioncolini et al. (2009a) as follows:

$$V_{lf}^+ = \frac{1}{\epsilon_{lf}^+}\left\{\frac{1}{1-\xi}\left[y^+ - \frac{y^{+2}}{2R^+} + \xi R^+ \ln\left(1-\frac{y^+}{R^+}\right)\right] + \frac{1}{2}C_{lf}y^{+2}\right\} \quad 0 \leqslant y^+ \leqslant t^+ \tag{22}$$

$$\xi = \frac{x^2G^2}{\varepsilon}\left|\frac{dv_g}{dP}\right|; \quad C_{lf} = \frac{y^{*2}}{\mu_l V^*}\left(\rho_l - \frac{\rho_l(1-\varepsilon)+\rho_g\varepsilon}{1-\xi}\right)g\sin\theta;$$
$$\epsilon_{lf}^+ = \sqrt{1+0.90\times10^{-3}t^{+2}} \tag{23}$$

where $v_g$ is the gas phase specific volume and $P$ the pressure. The dimensionless variables appearing in Eq. (22), together with the velocity $V^*$ and length $y^*$ scales, are defined as follows:

$$V_{lf}^+ = \frac{V_{lf}}{V^*}; \quad y^+ = \frac{y}{y^*}; \quad R^+ = \frac{R}{y^*}; \quad t^+ = \frac{t}{y^*}; \quad V^* = \sqrt{\frac{\tau_w}{\rho_l}}; \quad y^* = \frac{\mu_l}{\rho_l V^*} \tag{24}$$

Once the average liquid film thickness $t$ is known, the core flow diameter is simply calculated as $d_c = d - 2t$. This way of calculating the core flow diameter is generally more accurate than the estimate proposed in Eq. (10) and it is therefore preferred for the present analysis. Besides, evaluating the average liquid film thickness $t$ from differentiating the tube diameter $d$ and the core flow diameter $d_c$ would yield highly inaccurate estimates. The void fraction $\varepsilon$ and the liquid droplet hold-up $\gamma$ can be calculated from the following relations:

$$(1-\varepsilon)(1-\gamma)=\frac{t(2R-t)}{R^2};\quad \gamma\frac{1-\varepsilon}{\varepsilon}=e\frac{1-x}{x}\frac{\rho_g}{\rho_l} \tag{25}$$

where the left expression is derived from the liquid film flow area, while that on the right is derived by neglecting the slip between the carrier gas and the entrained droplets. Finally, the density $\rho_c$ and the viscosity $\mu_c$ of the droplet-laden gas core are calculated as follows:

$$\rho_c=(1-\varepsilon_c)\rho_l+\varepsilon_c\rho_g;\quad \mu_c=(1-\varepsilon_c)\mu_l+\varepsilon_c\mu_g;\quad \varepsilon_c=\frac{\varepsilon}{\varepsilon+\gamma(1-\varepsilon)} \tag{26}$$

where $\varepsilon_c$ is the droplet-laden gas core void fraction.

Returning to Eq. (19), application of dimensional analysis relates the entrained liquid fraction $e$ to the six dimensionless groups $\Pi_1$–$\Pi_6$ as follows:

$$e=e(\Pi_1,\Pi_2,\ldots,\Pi_6) \tag{27}$$

$$\begin{aligned}&\Pi_1=\frac{\rho_l}{\rho_c};\quad \Pi_2=\frac{\mu_l}{\mu_c};\quad \Pi_3=\frac{\rho_c V_c d_c}{\mu_c}=Re_c;\\ &\Pi_4=\frac{\rho_l V_l d_l}{\mu_l}=Re_l\quad \Pi_5=\frac{\rho_c V_c^2 d_c}{\sigma}=We_c;\quad \Pi_6=\frac{t}{d_c}\end{aligned} \tag{28}$$

The liquid film hydraulic diameter $d_l$ is calculated as:

$$d_l=4\frac{t}{d}(d-t) \tag{29}$$

A detailed derivation of the groups $\Pi_1$–$\Pi_6$ can be found in Cioncolini et al. (2009b) and is not repeated here. As can be seen, $\Pi_1$ and $\Pi_2$ are the ratios of the densities and viscosities of the liquid film and the gas core, respectively, $\Pi_3$ is a Reynolds number of the gas core, $\Pi_4$ is a Reynolds number of the liquid film, $\Pi_5$ is the core flow Weber number and $\Pi_6$ is the dimensionless liquid film thickness. The core flow Weber number $\Pi_5$, in particular, is the same group derived heuristically in Section 5 and used in Eqs. (17) and (18). Although the dimensionless groups $\Pi_1$–$\Pi_6$ are among the most frequently used in the annular two-phase flow literature, several other groups can be generated through manipulation of the equations, including the following:

$$\begin{aligned}&\Pi_7=\frac{\rho_l V_l t}{\mu_l};\quad \Pi_8=\frac{\rho_c V_c^2 t}{\sigma};\quad \Pi_9=\frac{\rho_c(V_c-V_l)^2 d_c}{\sigma};\\ &\Pi_{10}=\frac{\rho_l V_l^2 t}{\sigma};\quad \Pi_{11}=\frac{V_c}{V_l};\quad \Pi_{12}=\frac{\rho_c V_c^2}{\rho_l V_l^2};\\ &\Pi_{13}=\frac{\mu_l}{\sqrt{\rho_l\sigma t}};\quad \Pi_{14}=\frac{\mu_l V_l}{\sigma};\quad \Pi_{15}=\frac{\mu_c V_c}{\sigma}\end{aligned} \tag{30}$$

In particular, $\Pi_7$ and $\Pi_8$ are a Reynolds number for the liquid film and a Weber number for the core flow, respectively, with the average liquid film thickness $t$ as the characteristic dimension, $\Pi_9$ is an aerodynamic Weber number for the core flow with the relative velocity in place of the core velocity, $\Pi_{10}$ is a Weber number for the liquid film, $\Pi_{11}$ is the slip ratio, $\Pi_{12}$ and $\Pi_{13}$ are the momentum ratio and the Ohnesorge numbers, respectively, typically used in the study of sprays (Crowe, 2006), and finally $\Pi_{14}$ and $\Pi_{15}$ are capillary numbers for the liquid film and the gas core, respectively. In the present analysis, the acceleration of gravity $g$ is not included in the list of influential parameter in Eq. (19). Should the acceleration of gravity be included, following Oliemans et al. (1986), further dimensionless groups could be generated:

$$\Pi_{16}=\frac{V_c^2}{gd_c};\quad \Pi_{17}=\frac{V_l^2}{gt};\quad \Pi_{18}=\frac{\rho_c d_c^2 g}{\sigma};\quad \Pi_{19}=\frac{\rho_l t^2 g}{\sigma}; \tag{31}$$

where $\Pi_{16}$ and $\Pi_{17}$ are Froude numbers for the gas core and the liquid film, respectively, while $\Pi_{18}$ and $\Pi_{19}$ are Bond numbers for the gas core and the liquid film, respectively. Besides the set of dimensionless groups $\Pi_1$–$\Pi_6$ proposed in Eq. (28), different sets can be obtained by substituting one or more groups among $\Pi_1$–$\Pi_6$ with one or more groups picked among $\Pi_7$–$\Pi_{19}$, thus providing different correlating approaches. Returning to Eq. (27), a useful technique that can be used to check the degree of correlation between the entrained liquid fraction $e$ and the groups $\Pi_1$–$\Pi_6$ is multiple regression analysis. Here, in particular, a technique borrowed from statistical economics and applied in two-phase thermal–hydraulics for the first time by Stephan and Abdelsalam (1980) and also employed by Cioncolini et al. (2009b) is used. A first step in this approach is assuming a power law representation for Eq. (27) as follows:

$$e=e(\Pi_1,\Pi_2,\ldots,\Pi_6)=C\cdot\Pi_1^{a_1}\Pi_2^{a_2}\Pi_3^{a_3}\Pi_4^{a_4}\Pi_5^{a_5}\Pi_6^{a_6} \tag{32}$$

Then, the use of multiple regression analysis allows the values of the constant $C$ and exponents $a_1$–$a_6$ to be fixed that best fit the data and to provide a ranking of importance of the groups $\Pi_1$–$\Pi_6$, allowing selection of those groups that exert the most significant influence on $e$. Once the most influential groups are identified, if the power law representation is not flexible enough to satisfactorily fit the data, then more appropriate forms of correlating equations can be sought. More details on the actual implementation of this regression technique can be found in the literature cited, and are not repeated here.

The application of multiple regression analysis to the present databank, using the dimensionless groups $\Pi_1$–$\Pi_6$ and also the further groups $\Pi_7$–$\Pi_{19}$, identifies the core flow Weber number $\Pi_5$ as the most influential group in determining the entrained liquid fraction $e$, thus confirming the results of the preliminary heuristic analysis presented in Section 5. No other clear dependence is revealed, however, on any of the other groups considered. The aerodynamic core flow Weber number $\Pi_9$, in particular, although potentially more accurate than the core flow Weber number $\Pi_5$, is not found to provide any appreciable gain in accuracy. These findings by no means signify that the entrained liquid fraction depends only on the core flow Weber number. Rather, it is quite likely that the significant scatter in the available databank is large enough to hide any fine details in the data, so that only the predominant influence of the core flow Weber number clearly emerges, and any other second order dependence is lost. Within the limits of the present study, therefore, the use of dimensional analysis provides further support to the heuristic analysis already discussed but, unfortunately, does not allow further refinement of the correlation proposed. These findings clearly highlight the need to perform further experimental investigations on the entrained liquid fraction, possibly with improved experimental techniques to reduce the scatter in the data. Also, from Table 4 it can be seen that the majority of the available data are limited to $e<0.5$. Future experiments, therefore, should concentrate on the region of $e>0.5$, which is quite relevant for dryout prediction.

## 7. Conclusions

The performances of nine empirical correlations for use in predicting the entrained liquid fraction were evaluated with respect to a large experimental database compiled here for annular two-phase flow. Within the limits of the present study, the best predictions by an existing method are given by the correlations of Sawant et al. (2009) and Oliemans et al. (1986).

Using both physical intuition and dimensional analysis, the core flow Weber number was found to be the dominant dimensionless group in predicting the entrained liquid fraction. This same Weber

number already proved in a previous study to be the controlling dimensionless group in predicting the wall shear stress and the associated frictional pressure gradient of annular flows, so that this form of the Weber number seems capable of capturing a good deal of information regarding annular flows.

Further experimental investigations should concentrate on generating accurate data on the entrained liquid fraction, focusing in particular on annular flows with high entrained liquid fraction of interest for dryout predictions.

## Acknowledgements

The AERE Harwell databank was provided by Professor R.V.A. Oliemans, who is gratefully acknowledged. A. Cioncolini is supported by the Swiss National Science Foundation (SNSF) under Contract No. 200020-119651.

## Appendix A. Supplementary material

Supplementary data associated with this article can be found, in the online version, at doi:10.1016/j.ijmultiphaseflow.2009.11.011.

## References

Azzopardi, B.J., Zaidi, S.H., 2000. Determination of entrained fraction in vertical annular gas–liquid flow. ASME J. Fluids Eng. 122, 146–150.
Brown, D.J., 1978. Disequilibrium annular flow. Ph.D. Thesis, University of Oxford, Oxon.
Cioncolini, A., Thome, J.R., Lombardi, C., 2009a. Algebraic turbulence modeling in adiabatic gas–liquid annular two-phase flow. Int. J. Multiphase Flow 35, 580–596.
Cioncolini, A., Thome, J.R., Lombardi, C., 2009b. Unified macro-to-microscale method to predict two-phase frictional pressure drops of annular flows. Int. J. Multiphase Flow 35, 1138–1148.
Cousins, L.B., Hewitt, G.F., 1968a. Liquid phase mass transfer in annular two-phase flow: droplet deposition and liquid entrainment. Report AERE-R 5657, UKAEA, Harwell, Oxon.
Cousins, L.B., Hewitt, G.F., 1968b. Liquid phase mass transfer in annular two-phase flow: radial liquid mixing. Report AERE-R 5693, UKAEA, Harwell, Oxon.
Cousins, L.B., Denton, W.H., Hewitt, G.F., 1965. Liquid mass transfer in annular two-phase flow. In: Two-Phase Flow Symposium, Exeter, Devon, Paper C4.
Crowe, C.T., 2006. Multiphase Flow Handbook. CRC Press, Boca Raton, FL, USA.
Gill, L.E., Hewitt, G.F., Lacey, P.M.C., 1964. Sampling probe studies of the gas core in annular two-phase flow-II: studies of the effect of phase flow rates on phase and velocity distribution. Chem. Eng. Sci. 19, 665–682.
Gill, L.E., Hewitt, G.F., Roberts, D.N., 1969. Study of the behavior of disturbance waves in annular flow in a long vertical tube. Report AERE-R 6012, UKAEA, Harwell, Oxon.
Han, H., Gabriel, K.S., Wang, Z., 2007. A new method of entrainment fraction measurement in annular gas–liquid flow in a small diameter vertical tube. Flow Meas. Inst. 18, 79–86.
Hewitt, G.F., Pulling, D.J., 1969. Liquid entrainment in adiabatic steam–water flow. Report AERE-R 5374, UKAEA, Harwell, Oxon.
Hewitt, G.F., Roberts, D.N., 1969. Studies of two-phase flow patterns by simultaneous X-ray and flash photography. Report AERE-M 2159, HMSO, London.
Hinkle, W.D., 1967. A study of liquid mass transport in annular air–water flow. Ph.D. Thesis, Massachusetts Institute of Technology, Boston, USA.
Ishii, M., Mishima, K., 1989. Droplet entrainment correlation in annular two-phase flow. Int. J. Heat Mass Transfer 32, 1835–1846.
Jagota, A.K., Rhodes, E., Scott, D.S., 1973. Tracer measurements in two phase annular flow to obtain interchange and entrainment. Can. J. Chem. Eng. 51, 139–148.
Jepson, D.M., Azzopardi, B.J., Whalley, P.B., 1989. The effect of gas properties on drops in annular flow. Int. J. Multiphase Flow 15, 327–339.
Jukić, D., Scitovski, R., 1996. The existence of optimal parameters of the generalized logistic function. Appl. Math. Comput. 77, 281–294.
Keeys, R.K.F., Ralph, J.C., Roberts, D.N., 1970. Liquid entrainment in adiabatic steam–water flow at 500 and 1000 psia. Report AERE-R 6293, UKAEA, Harwell, Oxon.
Lopez de Bertodano, M.A., Assad, A., Beus, S.G., 2001. Experiments for entrainment rate of droplets in the annular regime. Int. J. Multiphase Flow 27, 685–699.
Mayinger, F., Langner, H., 1976. Steady state and transient entrainment behavior in upwards co-current annular flow. In: Proceedings of the 'NATO Advanced Study Institute on Two-Phase Flow and Heat Transfer', Istanbul, Turkey.
Minh, T.Q., Huyghe, J.D., 1965. Some hydrodynamical aspects of annular dispersed flow, entrainment and film thickness. In: Two-Phase Flow Symposium, Exeter, Devon, Paper C2.
Nakazatomi, M., Sekoguchi, K., 1996. Effect of pressure on entrainment flow rate in vertical upward gas–liquid annular two-phase flow. Part II: an assessment of published correlations of entrainment flow rate through high pressure data and proposal of new correlations. Heat Transfer Jpn. Res. 25, 281–292.
Nigmatulin, B.I., Malyshenko, V.I., Shugaev, Y.Z., 1977. Investigation of liquid distribution between the core and the film in annular dispersed flow of steam–water mixtures. Therm. Eng. 23, 66–68.
Okawa, T., Kotani, A., Kataoka, I., 2005. Experiments for liquid phase mass transfer rate in annular regime for a small vertical tube. Int. J. Heat Mass Transfer 48, 585–598.
Oliemans, R.V.A., Pots, B.F.M., Trompé, N., 1986. Modeling of annular dispersed two-phase flow in vertical pipes. Int. J. Multiphase Flow 12, 711–732.
Paleev, I.I., Filippovich, B.S., 1966. Phenomena of liquid transfer in two-phase dispersed annular flow. Int. J. Heat Mass Transfer 9, 1089–1093.
Pan, L., Hanratty, T.J., 2002. Correlation of entrainment for annular flow in vertical pipes. Int. J. Multiphase Flow 28, 363–384.
Reitz, R.D., Bracco, F.V., 1982. Mechanism of atomization of a liquid jet. Phys. Fluids 25, 1730–1742.
Sawant, P., Ishii, M., Mori, M., 2008. Droplet entrainment correlation in vertical upward co-current annular two-phase flow. Nucl. Eng. Des. 238, 1342–1352.
Sawant, P., Ishii, M., Mori, M., 2009. Prediction of amount of entrained droplets in vertical annular two-phase flow. Int. J. Heat Fluid Flow 30, 715–728.
Schadel, S.A., Leman, G.W., Binder, J.L., Hanratty, T.J., 1990. Rates of atomization and deposition in vertical annular flow. Int. J. Multiphase Flow 16, 363–374.
Sekoguchi, K., Tanaka, O., 1985. On the determination method of entrained droplet flow rate in the disturbance wave region of annular flow. Bull. JSME 28, 1105–1112.
Singh, K., St. Pierre, C.C., Crago, W.A., Moeck, E.O., 1969. Liquid film flow rates in two phase flow of steam and water at 1000 psia. AIChE J. 15, 51–56.
Stephan, K., Abdelsalam, M., 1980. Heat-transfer correlations for natural convection boiling. Int. J. Heat Mass Transfer 23, 73–87.
Utsuno, H., Kaminaga, F., 1998. Prediction of liquid film dryout in two-phase annular mist flow in a uniformly heated narrow tube: development of analytical method under BWR conditions. J. Nucl. Sci. Technol. 35, 643–653.
Wallis, G.B., 1962. The onset of droplets entrainment in annular gas–liquid flow. Report No. 62GL127, General Electric Co., Schenectady, NY.
Wallis, G.B., 1968. Phenomena of liquid transfer in two-phase dispersed annular flow. Int. J. Heat Mass Transfer 11, 783–785.
Whalley, P.B., Hewitt, G.F., Hutchinson, P., 1974. Experimental wave and entrainment measurements in vertical annular two-phase flow. In: Symposium Multi-Phase Flow Systems, University of Strathclyde, Scotland, Paper A1.
Woldesemayat, M.A., Ghajar, A.J., 2007. Comparison of void fraction correlations for different flow patterns in horizontal and upward inclined pipes. Int. J. Multiphase Flow 33, 347–370.
Wolf, A., Jayanti, S., Hewitt, G.F., 2001. Flow development in vertical annular flow. Chem. Eng. Sci. 56, 3221–3235.
Würtz, J., 1978. Entrainment in annular steam–water flow. In: European Two-Phase Flow Group Meeting, Stockholm, Sweden.